Available online at www.sciencedirect.com
ScienceDirect
Journal of the European Ceramic Society 28 (2008) 1535–1542
www.elsevier.com/locate/jeurceramsoc

Creep of monolithic and fibre-reinforced silicon carbide

B. Wilshire *, M.R. Bache

Materials Research Centre, School of Engineering, Swansea University, Singleton Park, Swansea SA2 8PP, United Kingdom

Available online 1 February 2008

Abstract

The mechanisms governing tensile creep and creep fracture are identified for siliconized silicon carbide (Si–SiC) and sintered silicon carbide (SSC), as well as for various SiC-matrix composites reinforced with interwoven bundles of different fibres. With Si–SiC and SSC, creep is controlled by the rate at which intergranular damage development allows grain boundary sliding. Fracture then results from the formation and link up of grain boundary cavities and cracks, unless premature failure occurs by rapid crack propagation from a pre-existing flaw. In contrast, with the woven SiC-matrix composites, immediate failure was never encountered on loading at stresses less than the UTS, despite the presence of macroscopic pores. Instead, the longitudinal fibres control the rates of creep strain accumulation and crack growth. However, the fracture properties are determined by oxidation-assisted fibre failure, because matrix cracking permits oxygen ingress during tests in air. By clarifying the processes limiting the creep capabilities of current product ranges, possible development avenues are suggested for fibre-reinforced composites displaying improved long-term service performance in oxidizing atmospheres.

Keywords: Composites; Fibres; Creep; Fracture; SiC

1. Introduction

At elevated temperatures, a number of high-melting point ceramics exhibit greater resistance to oxidation and chemical change, lower density, higher strength and elastic modulus than even the best nickel-base superalloys. Particularly for modern aeroengine applications, the successful development of ceramic components would then allow increased operating temperatures, resulting in improved efficiencies, lower specific fuel consumption and reduced emissions, without need for the intricate air cooling systems currently required with superalloys.[1,2] Yet, with operating lives of well over 10,000 h generally expected for civil engines, ceramic components must perform without failure for long periods under load at high temperatures in hostile atmospheres. Hence, good oxidation resistance must be combined with excellent creep and creep fracture strengths.

Of the available commercial materials, covalently bonded silicon carbide (SiC) and silicon nitride (Si_3N_4) are among the most creep resistant, with SiC offering superior temperature capability. However, for safety critical applications, component integrity is paramount, raising major concerns over the design constraints imposed by the inherently brittle nature of monolithic structural ceramics. Research emphasis has therefore been directed increasingly[3] to the development and assessment of ceramic-matrix composites (CMCs), particularly composites with improved toughness and damage tolerance achieved by reinforcement with continuous ceramic fibres (CFCMCs).

Although a wide variety of CFCMCs have been produced and evaluated, special attention has been focussed on composites with either SiC or Al_2O_3 matrices, incorporating interwoven bundles of silicon carbide fibres. Unfortunately, the creep strengths of these expensive composites at high temperatures are adversely affected in oxidizing environments,[4–6] as encountered in aeroengine service, so performance enhancement should be pursued along with product cost reduction.[1,2] For this reason, the present analysis summarizes the creep and creep fracture characteristics of silicon carbide ceramics, before considering ceramic–fibre-reinforced SiC-matrix composites with a view to identifying potential product development avenues.

2. Creep of silicon carbide ceramics

The high temperature creep properties of ceramics have usually been studied using compression or bend test procedures. However, with Si_3N_4 and SiC type ceramics, the creep strengths in tension can be an order of magnitude lower than in compression.[7–9] For most engineering applications, tensile

* Corresponding author. Tel.: +44 1792 295243; fax: +44 1792 295244.
E-mail address: b.wilshire@swansea.ac.uk (B. Wilshire).

0955-2219/$ – see front matter © 2007 Elsevier Ltd. All rights reserved.
doi:10.1016/j.jeurceramsoc.2007.12.008

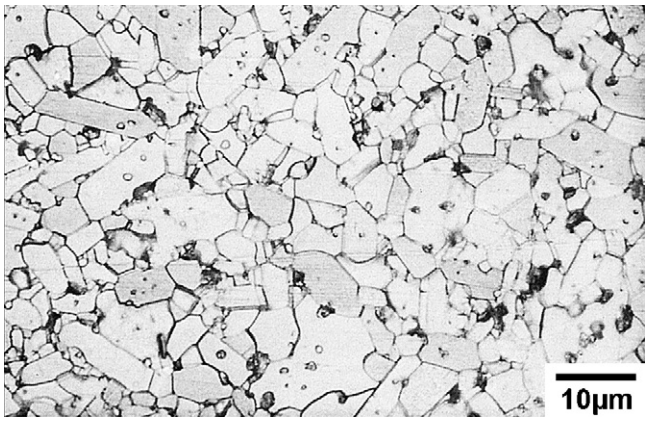

Fig. 1. Microstructure of as-produced sintered silicon carbide.[10].

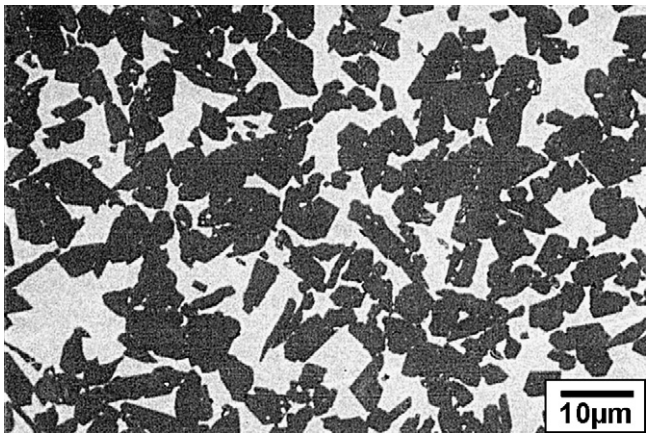

Fig. 2. Microstructure of siliconized silicon carbide containing 33 vol.% silicon, showing 5 μm grains of SiC and residual silicon12.[12].

stresses are life limiting, so only results obtained under tensile conditions are now featured.

The influence of microstructure and fabrication route on strain accumulation and damage evolution during tensile creep of silicon carbide ceramics can be illustrated by reference to data sets acquired[9,10] for siliconized silicon carbide (Si–SiC) and sintered silicon carbide (SSC). Details of these materials are given below:

(a) Solid state sintering of SiC, using boron or carbon as sintering aids, produces a polycrystalline product with SiC grains in direct contact, with no second phase present at the grain boundaries.[11] With the example shown in Fig. 1, the equiaxed grains had a mean 5–15 μm diameter, although some elongated crystals had an aspect ratio of 1:7 and a maximum dimension of 70 μm.[10] A uniform distribution of fine pores, together with an uneven distribution of larger voids (~10–100 μm diameter) and some metallic inclusions at triple points, were also evident.[10]

(b) Reaction-sintered Si–SiC is obtained by infiltration of molten silicon into carbonized partially bonded SiC. The silicon reacts with the carbon to form an interlocking structure of silicon carbide grains (~5 μm diameter), with residual silicon filling the remaining volume.[11] Substantial grain-to-grain bonding occurs with less than ~10 vol.% silicon, but the extent of direct bonding decreases on raising the silicon levels towards 33 vol.% (Fig. 2). The high-density Si–SiC is impermeable to oxygen and hence, resistant to internal oxidation at high temperatures.[11]

2.1. Creep property comparisons

Although the microstructures are markedly different (Figs. 1 and 2), several features of the tensile creep characteristics are similar for Si–SiC and SSC. For instance, as with most structural ceramics, the manner in which the creep strain (ε) accumulates with time (t) is comparable for both product types. Following the essentially elastic strain on loading, the creep rate ($\dot{\varepsilon} = d\varepsilon/dt$) decreases continuously with time throughout the decaying primary stage, approaching a minimum or secondary rate ($\dot{\varepsilon}_m$). In tension, failure then occurs after a time (t_f) at a strain (ε_f), such that $t = t_f$ when the accumulated strain reaches

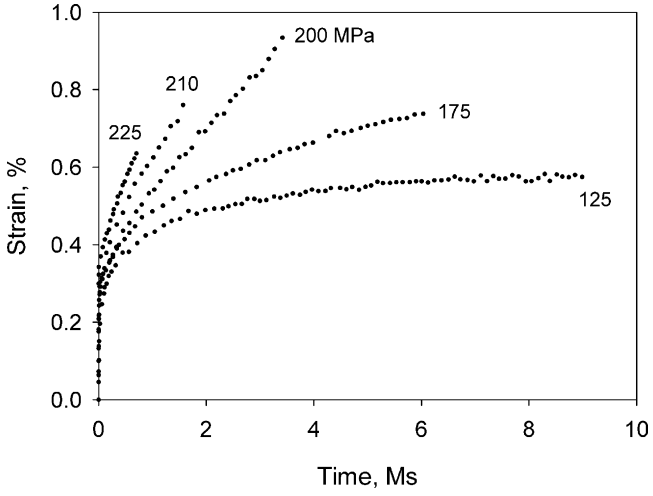

Fig. 3. Creep strain/time curves at tensile stresses from 125 MPa to 225 MPa for sintered silicon carbide [10] at 1500 °C.

the limiting creep ductility, i.e. when $\varepsilon = \varepsilon_f$. Thus, as illustrated in Fig. 3 for sintered silicon carbide,[10] fracture terminates the decaying creep curve with little or no accelerating tertiary stage. Yet, despite this distinctive creep curve shape, the creep properties of ceramics have generally been defined by monitoring only the $\dot{\varepsilon}_m$, t_f and ε_f values.

The creep rupture life increases and $\dot{\varepsilon}_m$ decreases as the stress (σ) and temperature (T) are reduced, with $\dot{\varepsilon}_m t_f$ falling from around 0.005 toward 0.002 as the test duration increases with sintered silicon carbide (Fig. 4), while $\dot{\varepsilon}_m t_f \cong 0.004$ for the various grades of Si–SiC.[12] Since the early 1950s, it has then become common practice to describe the stress dependences of $\dot{\varepsilon}_m$ and t_f using Norton's Law[13] as

$$\frac{M}{t_f} = \dot{\varepsilon}_m = A\sigma^n \tag{1}$$

where $M(= \dot{\varepsilon}_m t_f)$, but the parameter ($A$) and the stress exponent (n) are themselves functions of stress as well as temperature.

Using Eq. (1), the $\log \dot{\varepsilon}_m / \log \sigma$ plots for silicon carbide and silicon nitride products may be better represented by continuous curves, but these relationships are generally approximated

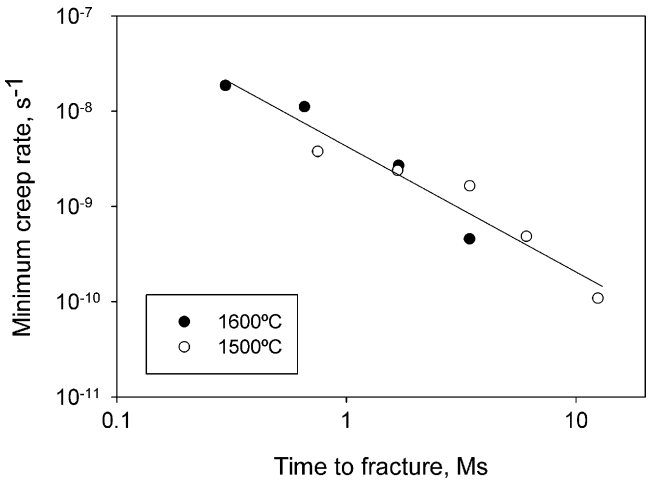

Fig. 4. The dependence of the creep life on the minimum creep rate for sintered silicon carbide [10] at 1500 °C and 1600 °C.

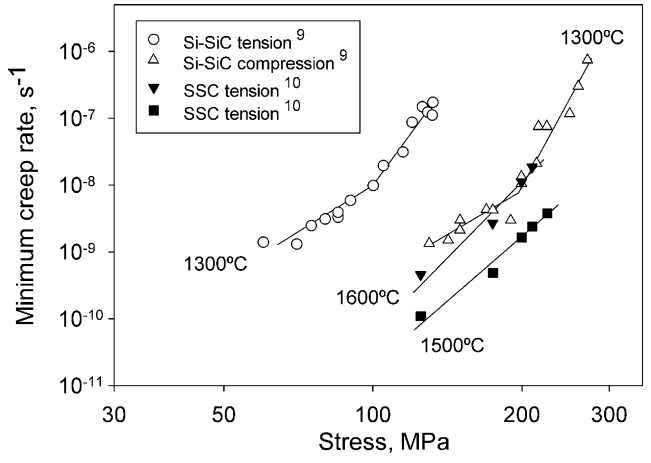

Fig. 5. The stress dependences of the minimum creep rate in tension and compression at 1300 °C for the siliconized silicon carbide [11] shown in Fig. 2 and in tension at 1500 °C and 1600 °C for the sintered silicon carbide [10] shown in Fig. 1.

by a series of straight-line segments (Fig. 5). Thus, a gradient decrease from $n \cong 12$ to $n \cong 4$ has been reported for Si–SiC as the applied stress is reduced,[9] whereas $n \cong 7$ over the stress-temperature ranges covered for SSC.[10] Inspection of the results in Fig. 5 then confirms that, at the same applied stress,

(a) the creep rates recorded for Si–SiC in tension are several orders of magnitude faster than in compression [9] and
(b) the tensile creep rates determined for SSC testpieces[10] at 1500 °C are lower than even the compressive rates noted for Si–SiC[9] at 1300 °C, demonstrating the excellent creep strength of sintered silicon carbide. Even so, 25% of all SSC specimens failed immediately on loading over the entire stress-temperature range investigated.[10]

2.2. Creep deformation and damage processes

Using power law expressions Eq. (1), changes in n value are widely attributed to transitions in the dominant creep process,[14–16] e.g. dislocation processes ($n > 3$), grain boundary sliding ($n \cong 2$), diffusional creep mechanisms ($n \cong 1$). However, after almost half a century of endeavour with both metallic and ceramic materials, no general agreement has been reached on the detailed processes involved, particularly when $n \rightarrow 1$ at low stresses[17] and when $n > 4$ at high stresses,[18] as in Fig. 5.

One basic problem with creep mechanism identification stems from the fact that most creep theories have attempted to account for secondary or 'steady state' behaviour but, for a wide range of materials, a 'steady state' rarely exists.[19,20] Instead, when normal creep curves are displayed, only a minimum rate ($\dot{\varepsilon}_m$) is found when the decaying primary rate is offset by the tertiary acceleration. On this basis, creep behaviour patterns should be discussed in terms of the processes governing strain accumulation and the various damage phenomena affecting the tertiary acceleration and eventual failure. But, it then becomes necessary to explain why substantial damage evolution (Fig. 6) terminates the decaying creep curve without initiating a definitive tertiary stage with SSC (Fig. 3), as well as with various Si–SiC and Si_3N_4 type ceramics.

With highly covalent SiC and Si_3N_4 products, creep cannot take place by the movement of lattice dislocations, even at temperatures over 1577 °C. So, with essentially non-deforming grains, creep properties are commonly interpreted by invoking processes dependent on the presence of intergranular phases which are viscous at the creep temperatures, including

- relative grain movement controlled by the viscosity of the grain boundary phase,
- viscous phase transfer from boundaries under compression to those under tension and
- solution/redeposition of grain material transported through the viscous phase.

Although intergranular viscous phases are frequently present, such phases are ultra-thin or absent with sintered silicon carbide.[11] It therefore appears that, with SSC and many other silicon carbide and silicon nitride ceramics, the creep rate at any instant is determined by the rate at which grain boundaries decohere to allow relative movement (sliding) of adjacent crystals.[8]

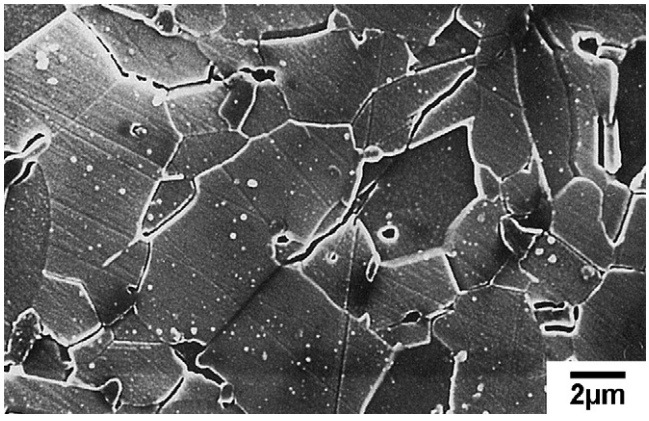

Fig. 6. Intergranular damage development during creep of sintered silicon carbide [10] in air under an applied stress of 210 MPa at 1500 °C.

Cavities and cracks nucleate first at boundaries with the weakest grain-to-grain bonding oriented approximately normal to the tensile stress axis, with the primary creep rate decreasing continuously as cracking must subsequently occur on more strongly bonded boundaries with a less favourable orientation. The damage incidence then increases more slowly with time, accounting for much of the primary strain, until failure occurs when cavity and crack link up creates a dominant crack of a critical size for the imposed stress-temperature conditions.

Of course, the creep properties and even the dominant deformation processes are material, microstructure and test condition sensitive. With Si–SiC containing less than 10 vol.% silicon, the deformation processes appear to be same as with SSC [11] but, with reduced grain-to-grain bonding, the creep resistance of Si–SiC is lower than SSC (Fig. 5). As the volume of more easily deformed silicon increases towards 33 vol.%, the decrease in bonding between SiC grains results in a progressive reduction in creep strength.[11]

2.3. Creep fracture characteristics

The idea that creep is controlled by the rate at which intergranular damage development allows grain boundary sliding also explains the strength differences observed for SiC and Si_3N_4 type ceramics in tension and compression. If the creep rates were determined by lattice processes, diffusional creep mechanisms or models dependent on a viscous boundary phase, comparable creep rates would be expected in tension and compression under the same stress-temperature conditions. However, the formation of intergranular cracks depends on the tensile stress normal to the boundary. In a compression test, finite element modelling has established that the maximum tensile hoop and radial stresses are only about a tenth of the applied compressive stress,[21] accounting for results of the type shown for Si–SiC in Fig. 5.

Although the sintered silicon carbide generally failed through the formation and link up of intergranular cavities and cracks (Fig. 6), when premature failure occurred on loading,[10] fracture was invariably a consequence of rapid growth of a crack originating at a pre-existing void (Fig. 7). As reported for structural ceramics in general[22] and Si–SiC in particular,[9] two modes of creep failure may therefore be displayed, namely, gradual development of intergranular damage or rapid crack propagation from a pre-existing dominant flaw.

The risk of a dominant flaw must increase as the component size increases but, even if the fabrication routes can avoid incomplete sintering and the creation of other critical defects, a further complication affects the use of monolithic SiC ceramics for structural applications. Specifically, the absence of an accelerating tertiary stage defines creep–brittle behaviour, i.e. $\varepsilon_f/\varepsilon_p \cong 1$, where ε_p is the primary creep strain. This lack of creep ductility can also be quantified through the relationship between $\dot{\varepsilon}_m t_f$ and ε_f as

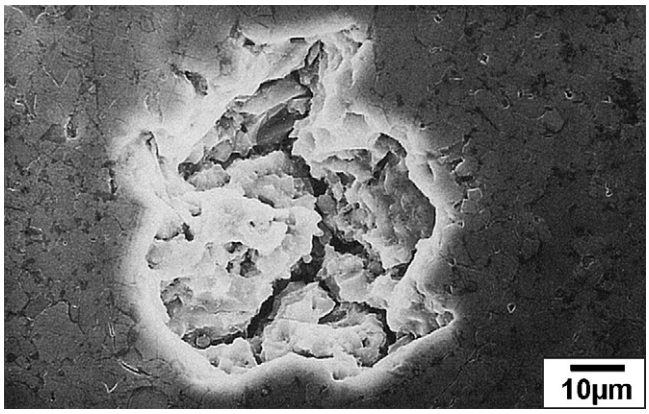

Fig. 7. Appearance of a large pre-existing void in sintered silicon carbide.[10]

$$\lambda = \varepsilon_f/\dot{\varepsilon}_m t_f \quad (2)$$

where λ is the creep damage tolerance parameter.[23] The λ value is important in practical situations, with $\lambda > 5$ thought to avoid premature cracking at local strain concentrations during service, say, where a change in component cross-section leads to stress concentrations.

At 1500 and 1600 °C with SSC,[10] $\varepsilon_f \cong 0.006$ to 0.011 over stress ranges giving creep lives up to almost 4000 h (1.44×10^7 s), with ε_f increasing from around 0.006 to about 0.014 as the test duration increases at 1300 °C to 1400 °C with Si–SiC.[9] Even though the $\dot{\varepsilon}_m t_f$ values are also low for these materials (Fig. 4), $\lambda < 5$ with Eq. (2). Yet strictly, because damage development normally affects the tertiary not the primary behaviour, Eq. (2) should be replaced by[24]

$$\lambda = [1 + (\varepsilon_t/\dot{\varepsilon}_m t_f)] \quad (3)$$

where ε_t is the total tertiary strain so, with $\varepsilon_t \cong 0$, $\lambda \cong 1$. Thus, monolithic silicon carbide and all related materials are not creep damage tolerant, with the need to avoid this design limitation justifying the development of ceramic-matrix composites.

3. Creep of fibre-reinforced SiC-matrix composites

Creep property comparisons have already been carried out for a wide range of CFCMCs with different fibres, matrices and fibre/matrix interfaces.[24,25] Hence, only the major con-

Table 1
Distinguishing features of SiC-fibre-reinforced SiC-matrix composites

Material designation	Fibre type	Matrix material	Interface type	Ref
SiC_f–SiC	Nicalon™ NLM 202	SiC	Carbon	26,29
SiC_f–SIBC	Nicalon™ NLM 202	Enhanced SiC	Carbon	27
$HNSiC_f$–SiC	Hi-Nicalon™	SiC	Carbon	28
$HNSiC_f$–SiBC	Hi-Nicalon™	Enhanced SiC	Carbon	24

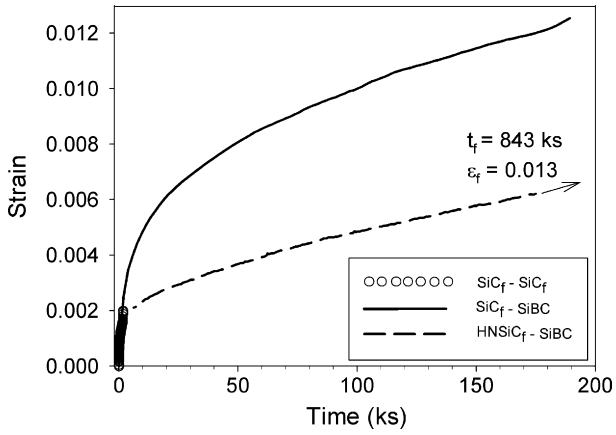

Fig. 8. Creep strain/time curves recorded for SiC_f–SiC [29] and SiC_f–SiBC [27] at 90 MPa and a $HNSiC_f$–SiBC specimen [24] at 100 MPa for tensile tests in air at 1300 °C.

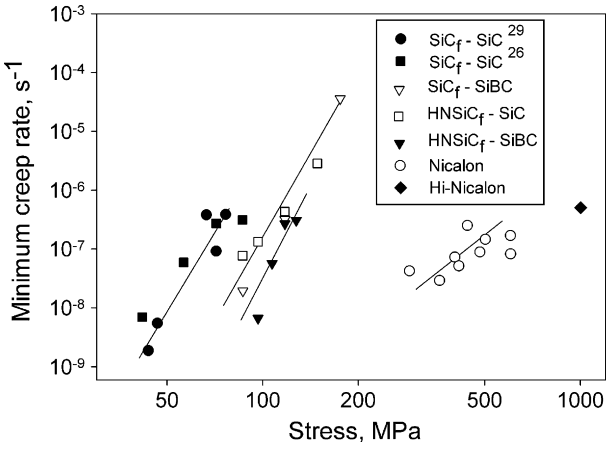

Fig. 9. The stress dependences of the minimum creep rates recorded for SiC_f–SiC,[26,29] SiC_f–SiBC,[27] $HNSiC_f$–SiC [28] and $HNSiC_f$–SiBC,[24] as well as for Nicalon™ NLM 202[33] and Hi-Nicalon™ fibres [31] at 1300 °C.

clusions of these studies are now summarized in an attempt to identify potential ways of overcoming the principal creep-life-limiting features of the SiC-matrix composites. For this purpose, the present analyses are based largely on the creep behaviour patterns reported[24–29] for the four CFCMCs listed in Table 1.

The SiC-matrix composites were reinforced with two types of SiC fibre, namely, Nicalon™ NLM 202 or Hi-Nicalon™ (Nippon Carbon Co., Japan). Hi-Nicalon™ fibres display superior elastic moduli and creep resistance, achieved by eliminating the amorphous silicon oxy-carbide phase (SiC_xO_y) which reduces the creep strength of Nicalon™ NLM 202 fibres.[30,31] These fibres reinforced either 'standard' or 'enhanced' SiC matrices, both produced by chemical vapour infiltration, but the 'enhanced' material contained boron-based additives which form a sealant glass to limit oxygen ingress during creep in oxidizing atmospheres.[32]

In all cases, the composites were manufactured with approximately 40 vol.% of carbon-coated fibres with average diameters of ~15 μm, incorporated as bundles of about 500 fibres woven to obtain 2D layers of fabric. The woven plies were aligned and stacked to give preforms having a balanced 0/90° architecture. After fibre coating and densification, the matrices had porosities of 15% or more, present as small pores within the fibre bundles and as macro-pores between the plies and at yarn intersections within the plies. For brevity, the four products are designated as $HNSiC_f$–SiC, $HNSiC_f$–SiBC, SiC_f–SiC and SiC_f–SiBC in Table 1.

To be relevant to aeroengine service, all results now quoted for the four composites[24–29] were determined in air at 1300 °C under tensile creep conditions.

3.1. Relative creep strengths of fibres and matrices

As found[10] for SSC (Fig. 3) and Si–SiC,[9] as well as for Nicalon™ NLM 202[33] and Hi-Nicalon™ fibres,[31] the ε/t trajectories for all composites listed in Table 1 reveal that the creep rate decays continuously to a minimum rate, again with little or no accelerating tertiary period before fracture (Fig. 8). From the ε/t curves, the values of $\dot{\varepsilon}_m$, t_f and ε_f were determined to show the stress dependences of $\dot{\varepsilon}_m$ (Fig. 9), the variations of t_f with $\dot{\varepsilon}_m$ (Fig. 10) and the relationship between $\dot{\varepsilon}_m t_f$ and ε_f (Fig. 11).

Data sets of the type presented in Figs. 8–11 have often been discussed by considering the relative creep strengths of the fibres and matrices.[34,35] Thus, for example, it was suggested that the creep properties of the SiC_f–SiC,[26] SiC_f–SiBC[27] and $HNSiC_f$–SiC products[28] are controlled by the stronger matrices. However, for a broad range of CFCMCs with various SiC or Al_2O_3 fibres reinforcing SiC, SiBC or Al_2O_3 matrices, the creep resistance of the fibre was always greater than that of the weak porous matrix.[25] This statement is verified by the results documented in Fig. 9. Clearly to achieve the same creep rate, the stress applied to the composite is only about one fifth of that required with the relevant Nicalon™ NLM 202 or Hi-Nicalon™ fibres. This outcome would be expected because the composites contain about 40 vol.% of interwoven fibre bundles, so the fibres parallel to the tensile stress axis occupy approximately one fifth of the testpiece cross-sectional area. Hence, the load-bearing

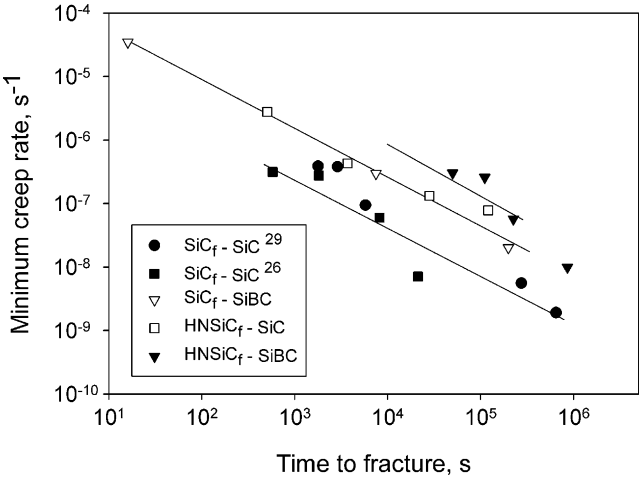

Fig. 10. The dependences of the creep rupture lives on the minimum creep rates for SiC_f–SiC,[26,29] SiC_f–SiBC,[27] $HNSiC_f$–SiC [28] and $HNSiC_f$–SiBC [24] in air at 1300 °C.

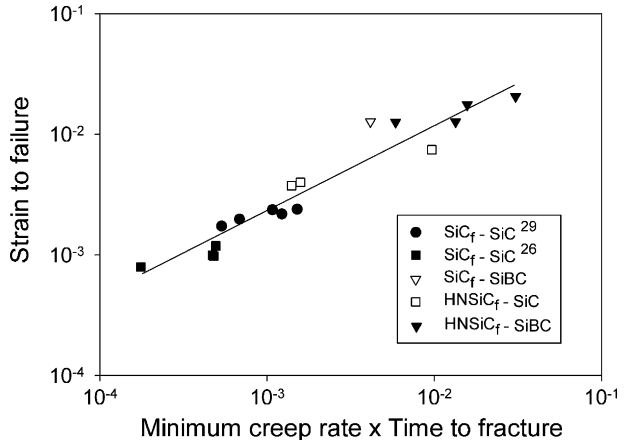

Fig. 11. The relationships between the product, $\dot{\varepsilon}_m t_f$, and the creep ductility (ε_f) for SiC_f–SiC,[26,29] SiC_f–SiBC,[27] $HNSiC_f$–SiC [28] and $HNSiC_f$–SiBC [24] in air at 1300 °C.

capabilities of the composite are governed by the longitudinal (0°) fibres.

The same conclusion was reached from a detailed comparison[29] of the relative creep strengths of polycrystalline alumina and alumina-matrix composites reinforced with either 25 vol.% SiC whiskers or 40 vol.% SiC fibres. Even so, with the matrices contributing little to the composite strengths, it then becomes necessary to explain why replacing the standard SiC-matrix with enhanced SiBC significantly improves the creep resistance of CFCMCs produced with the same volume fraction of Nicalon™ NLM 202 or Hi-Nicalon™ fibres (Fig. 9).

3.2. Creep in oxidizing atmospheres

The deformation and damage processes governing the tensile creep properties of SiC-fibre-reinforced SiC-matrix composites are now summarized, providing a framework to account for the improvements in the strength of standard SiC_f–SiC by changing the fibre and/or matrix (Figs. 8–11).

On applying a tensile load to a 'textile' CFCMC, the interwoven longitudinal fibre bundles extend and straighten in the stress direction. The weakest fibre regions deform most easily, so the high initial creep rates decay as load is transferred to the stronger bundles. The resulting complex stress state then leads to matrix crack formation within and between the 0° and 90° fibre tows. These 'tunnelling' cracks by-pass fibres in the 90° bundles but, on penetrating into the 0° bundles, the cracks become bridged by unbroken longitudinal fibres. Cracks can therefore open and extend only at rates determined by the creep resistance of the bridging fibres. Eventually, crack growth and link up produces a 'macro-crack' capable of propagating rapidly along planes normal to the tensile axis, with final failure accompanied by fibre pull out (Fig. 12). Fibre control of the creep resistance and crack growth rates then explains the dependence of t_f on $\dot{\varepsilon}_m$ (Fig. 10) and the performance improvement realized by replacing the Nicalon™ with Hi-Nicalon™ fibres (Figs. 9 and 10).

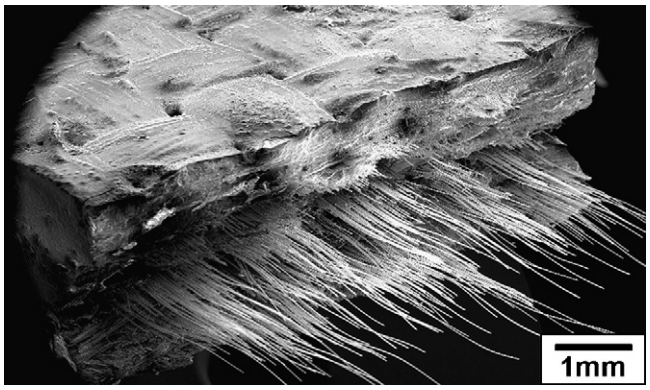

Fig. 12. Scanning electron micrograph showing regions of fibre pull out on the fracture surface of SiC_f–SiC [29] tested in air at 1300 °C.

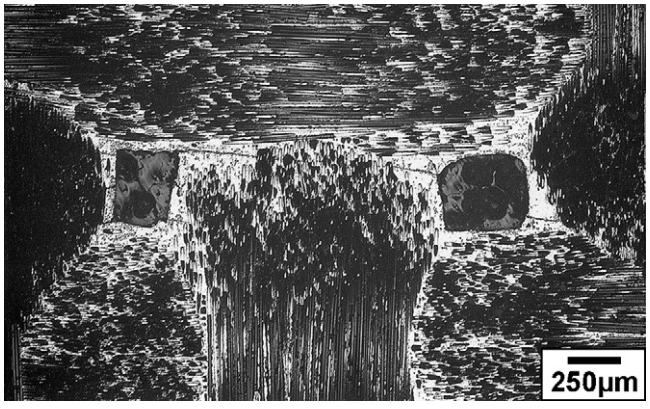

Fig. 13. Scanning electron micrograph showing link up of cracks nucleating at adjacent surface macro-pores [29] during creep of SiC_f–SiC in air at 1300 °C.

With standard SiC_f–SiC, a dominant crack nucleates at surface macro-pores (Fig. 13) with direct oxygen penetration along the crack resulting in failure of the crack-bridging fibres. The resulting low ductilities ensure early termination of the decaying creep curves, giving high $\dot{\varepsilon}_m$ and low t_f values (Fig. 8). Limiting oxygen ingress by the boron based sealant glass then lowers the rate of oxidation-assisted fibre failure, increasing the ductility by postponing fracture (Fig. 8). In this way, $\dot{\varepsilon}_m$ is reduced (Fig. 9) and t_f correspondingly raised (Fig. 10) by replacing the standard SiC-matrix with enhanced SiBC.

The creep strengths of standard SiC_f–SiC type composites are therefore improved substantially by reinforcing enhanced SiBC matrices with Hi-Nicalon™ fibres (Figs. 8–10). Yet, even with the high-performance $HNSiC_f$–SiBC product, the variation in $\dot{\varepsilon}_m t_f$ and ε_f in Fig. 11 indicates that $\lambda < 2$ using Eq. (2) but, with no significant tertiary stage, $\lambda = 1$ with Eq. (3). Because relatively large creep cracks and macro-pores can exist without causing immediate failure of the woven SiC-fibre-reinforced composites, these materials can therefore be regarded as crack tolerant but not creep damage tolerant.

3.3. Possible composite development avenues

For the same volume fraction and architecture of Nicalon™ or Hi-Nicalon™ fibres, similar creep properties are recorded

for composites with enhanced SiBC matrices and 0.5 μm thick carbon interfaces and with Al_2O_3 matrices having 5 μm thick SiC/BN interfaces.[25] Yet, the SiC_f–Al_2O_3 products also failed as a consequence of oxidation-assisted fibre attack. Indeed, this fracture mode is dominant even with CFCMCs reinforced with oxide fibres. Thus, with a SiC-matrix product reinforced with 40 vol.% of woven carbon-coated alumina fibre bundles (termed Al_2O_{3f}–SiC), a dramatic fall in creep ductility and strength was reported on changing the test atmosphere from vacuum to air.[36]

These observations indicate that, in oxidizing environments, even oxide–oxide composites may be prone to failure of the vulnerable interfaces and fibres. In addition, the upper temperature limits of SiC fibres are significantly higher than with currently available oxide fibres.[37] Hence, two new product options are now suggested, recognizing that the value of the suggestions must depend on economic fabrication routes being evolved to produce the composites satisfactorily.

(a) Among the different processing options for manufacture of carbon-fibre-reinforced silicon carbide (C_f–SiC), liquid silicon infiltration of porous carbon preforms under vacuum at around 1450 °C is one of the fastest and most cost-effective.[38,39] However, if SiC fibre reinforcement is preferred, a study has been made of the room temperature mechanical properties of four BN/SiC-coated SiC fibre performs before and after different time–temperature exposures in 0.1 MPa argon atmospheres.[40] The four types of SiC fibre were Hi-Nicalon™ and Hi-Nicalon-S™ from Nippon Carbon Co., as well as Sylramic™ from the Dow Corning Co. and in situ BN-coated Sylramic™ produced by a NASA process.[40] While the Hi-Nicalon™ type fibres were stable only up to 1400 °C, the Sylamic™ and stronger in situ Sylamic™ products retained their as-received strengths after 1 h at 1800 °C and after 100 h at 1600 °C. Sylramic™ type performs could then be partially densified with carbon or carbonized silicon carbide before impregnating with molten silicon, potentially forming a dense matrix with retained silicon to give the freedom from oxygen penetration and internal oxidation reported for siliconized silicon carbide.[11]

(b) A more radical alternative relies on the impressive creep strengths noted in tests carried out under low-pressure argon for a SiC-matrix composite, having the carbon fabric layers interlinked to give a material designated as 2.5 D C_f–SiC.[41,42] However, as with the Al_2O_{3f}–SiC samples,[36] a major reduction in creep life and ductility would be expected when crack development in the brittle SiC-matrix allows oxygen ingress to cause failure of the carbon fibres in non-protective atmospheres. Yet, intergranular cavities and cracks are found during creep of single-phase MgO and CaO but not with doloma (i.e. two-phase CaO–MgO containing ~42–50% MgO), indicating that damage forms on CaO–CaO and MgO–MgO boundaries rather than CaO–MgO interfaces.[43,44] Provided that low porosity doloma matrices can be produced free of interconnected pores that allow oxygen ingress, the creep strengths displayed by C_f–SiC in argon[41,42] may be attainable with C_f–doloma composites in oxidizing atmospheres.[24]

4. Conclusions

As with most structural ceramics, sintered and siliconized silicon carbide display continuously decaying creep curves, i.e. the primary creep rate decreases continuously towards a minimum rate, with little or no accelerating tertiary period evident before fracture. With these SiC ceramics, creep failure is a consequence of the progressive development and eventual link up of grain boundary cavities and cracks, unless fracture occurs immediately on loading by propagation of a crack originating at a pre-existing void or flaw. The risk of dominant flaws, plus the inherent lack of creep damage tolerance, therefore represents a service engineering design constraint.

Results are also analysed for various ceramic–fibre-reinforced SiC-matrix composites having different fibres, matrices and macro-pore distributions, which were fabricated and tested in different laboratories. Yet, the observed behaviour patterns are remarkably consistent, with failure never encountered immediately on loading, despite the presence of large pre-existing macro-pores. With these woven CFCMCs, the longitudinal fibres control the rates of creep strain accumulation and crack growth but for tests in air, the creep ductilities and rupture lives are determined by fibre failure caused by oxygen penetration as matrix cracks form. Even so, large cracks can exist prior to failure, but no accelerating tertiary stage precedes fracture, so these materials can be regarded as crack tolerant but not creep damage tolerant.

The creep performance of SiC_f–SiC type composites is increased by using high-strength Hi-Nicalon™ fibres to reinforce matrices which limit oxygen ingress, such as enhanced silicon carbide. With the aim of minimizing the life-limiting problem of oxidation-assisted fibre failure, suggestions are then made for fibre/matrix combinations which could offer the prospect of improved creep damage resistance for high temperature applications involving long-term service under load in oxidizing environments.

References

1. Ruffles, P., *Aerospace Structural Materials: Present and Future*. The Institute of Materials, London, 1995.
2. Miller, S., Advanced materials means advanced engines. *Interdiscip. Sci. Rev.*, 1996, **21**, 2–18.
3. Evans, A. G., Perspectives on the development of high-toughness ceramics. *J. Am. Ceram. Soc.*, 1990, **73**, 187–206.
4. Heredia, F. E., McNulty, J. C., Zok, F. W. and Evans, A. G., Oxidation embrittlement probe for ceramic-matrix composites. *J. Am. Ceram. Soc.*, 1995, **78**, 2097–3001.
5. Jones, R. H., Henager Jr., C. H. and Windish Jr., C. F., High temperature corrosion and crack growth of SiC–SiC at variable oxygen partial pressures. *Mater. Sci. Eng. A*, 1995, **A198**, 103–112.
6. Wilshire, B., Carreño, F. and Percival, M. G. L., Tensile creep and creep fracture of a fibre-reinforced SiC–SiC composite. *Scripta Mater.*, 1998, **39**, 729–732.

7. Kossowsky, R., Millar, D. J. and Diaz, E. S., Tensile and creep strengths of hot-pressed Si_3N_4. *J. Mater. Sci.*, 1975, **10**, 986–998.
8. Birch, J. M., Godfrey, D. J. and Wilshire, B., Deformation and fracture processes during creep of reaction bonded and hot pressed silicon nitride. *Proc. Br. Ceram. Soc.*, 1978, **26**, 141–154.
9. Wiederhorn, S. M., Roberts, D. E., Chuang, T. J. and Chuck, L., Damage enhanced creep in siliconized silicon carbide: phenomenology. *J. Am. Ceram. Soc.*, 1988, **71**, 602–608.
10. Wilshire, B. and Jiang, H., Deformation and failure processes during tensile creep of sintered silicon carbide. *Br. Ceram. Trans.*, 1994, **93**, 213–218.
11. Wiederhorn, S. M., Non-oxide ceramics, creep and creep rupture of silicon nitrides and silicon carbides. In *Encyclopaedia of Materials: Science and Technology*, ed. K. H. J. Buschaw, R. W. Cahn, M. C. Flemings, B. Ilschner, E. J. Kramer and S. Mahajan. Elsevier, Amsterdam, 2001, pp. 6283–6284.
12. Wiederhorn, S. M., Fields, B. A. and Hockey, B. J., Fracture of silicon nitride and silicon carbide at elevated temperatures. *Mater. Sci. Eng. A*, 1994, **A176**, 51–60.
13. Norton, F. H., *The Creep of Steels at High Temperature*. McGraw-Hill, New York, 1929.
14. Evans, A. G. and Langdon, T. G., Structural ceramics. *Prog. Mater. Sci.*, 1976, **21**, 171.
15. Davies, R. F. and Carter Jr., C. H., A review of creep in silicon nitride and silicon carbide. In *Advanced Ceramics*, ed. S. Saito. Oxford University Press, Oxford, 1988, pp. 95–125.
16. Hynes, A. and Doremus, R., Theories of creep in ceramics. *Crit. Rev. Solid State Mater.*, 1996, **21**, 129–187.
17. Mishra, R. S., Mukherjee, A. K. and Murty, K. L., ed., *Creep Behaviour of Advanced Materials for the 21st Century*. TMS, Warrendale, PA, 1999, pp. 391–507.
18. Arzt, E., Creep of dispersion strengthened materials: a critical assessment. *Res. Mech.*, 1991, **31**, 399–453.
19. Evans, R. W. and Wilshire, B., *Creep of Metals and Alloys*. The Institute of Metals, 1985.
20. Evans, R. W. and Wilshire, B., The θ approach to creep of structural ceramics. *Rev. Powder Metall. Phys. Chem*, 1992, **5**, 111–168.
21. Birch, J. M., Wilshire, B., Owen, D. R. J. and Shantaram, D., The influence of stress distribution on the deformation and fracture behaviour of ceramic materials under compressive creep conditions. *J. Mater. Sci.*, 1976, **11**, 1817–1825.
22. Evans, A. G. and Dagleish, B. J., Some aspects of the high temperature performance of ceramics and ceramic composites. In *Creep and Fracture of Engineering Materials and Structures*, ed. B. Wilshire and R. W. Evans. The Institute of Metals, London, 1987, pp. 929–955.
23. Leckie, F. A. and Hayhurst, D. R., Constitutive equations for creep rupture. *Acta Metall.*, 1977, **25**, 1059–1070.
24. Wilshire, B. and Bache, M. R., Creep damage resistance of ceramic-matrix composites. *J. Eur. Ceram. Soc.*, 2007, **27**, 4603–4611.
25. Wilshire, B., Creep property comparisons for ceramic–fibre-reinforced ceramic-matrix composites. *J. Eur. Ceram. Soc.*, 2002, **22**, 1329–1337.
26. Zhu, S., Mizuno, M., Kagawa, Y., Cao, J., Nagano, Y. and Kaya, H., Creep and fatigue behaviour of SiC fibre reinforced SiC composite at high temperatures. *Mater. Sci. Eng.*, 1997, **A225**, 69–77.
27. Zhu, S., Mizuno, M., Nagano, Y., Cao, J., Kagawa, Y. and Kaya, H., Creep and fatigue behaviour of an enhanced SiC–SiC composite at high temperatures. *J. Am. Ceram. Soc.*, 1998, **81**, 2269–2277.
28. Zhu, S., Mizuno, M., Kagawa, Y., Cao, J., Nagano, Y. and Kaya, H., Creep and fatigue behaviour in Hi-Nicalon Trade Mark-fibre-reinforced silicon carbide composites at high temperatures. *J. Am. Ceram. Soc.*, 1999, **82**, 117–128.
29. Wilshire, B. and Carreño, F., Deformation and damage processes during tensile creep of ceramic–fibre-reinforced ceramic-matrix composites. *J. Eur. Ceram. Soc.*, 2000, **20**, 463–472.
30. Bodet, R., Bourrat, X., Lamon, J. and Naslain, R., Tensile creep behaviour of a silicon-carbide-based fibre with a low oxygen content. *J. Mater. Sci.*, 1995, **30**, 661–677.
31. Challon, G., Pailler, R., Naslain, R. and Olry, P., Correlation between microstructure and mechanical behaviour at high temperatures of a SiC fibre with a low oxygen content (Hi-Nicalon). *J. Mater. Sci.*, 1997, **32**, 1133–1147.
32. Fox, D. S. and Nguyan, Q. N., Oxidation kinetics of enhanced SiC–SiC. *Ceram. Eng. Sci. Proc.*, 1995, **16**, 877–884.
33. Simon, G. and Bunsell, A. R., Creep behaviour and structural characterization at high temperature of Nicalon Trade Mark SiC fibres. *J. Mater. Sci.*, 1984, **19**, 3658–3670.
34. Evans, A. G. and Weber, C., Creep damage in SiC/SiC composites. *Mater. Sci. Eng. A.*, 1996, **A208**, 1–6.
35. Chermant, J. L. and Holmes, J., Elevated temperature creep and cyclic creep behaviour of fibre-reinforced ceramics. *Ceram. Trans.*, 1995, **57**, 95–103.
36. Lamouroux, F., Steen, M. and Vallés, J. L., Damage of a 2D Al_2O_3–SiC composite during uniaxial creep. *Comp. Sci. Technol.*, 1996, **56**, 825–830.
37. Parlier, M. and Ritti, M. H., State of the art and perspectives for oxide–oxide composites. *Aerospace Sci. Technol.*, 2003, **14**, 1–11.
38. Műller, M., Mentz, J., Buchkremer, H. P. and Stöver, D., Origin and effect of fibre attack for the processing of C/SiC. In *High Temperature Ceramic Matrix Composites*, ed. E. Krenkel, R. Naslain and H. Schneider. Wiley–VCH, Weinheim, 2001, pp. 66–72.
39. Kochendörfer, R. and Lützenburger, N., Applications of CMCs made via the liquid silicon infiltration (LSI) technique. In *High Temperature Ceramic Matrix Composites*, ed. E. Krenkel, R. Naslain and H. Schneider. Wiley–VCH, Weinheim, 2001, pp. 277–287.
40. Bhatt, R. T., Influence of high temperature argon heat treatment on tensile properties of four types of BN/SiC-coated SiC fiber preforms. In *High Temperature Ceramic Matrix Composites*, ed. E. Krenkel, R. Naslain and H. Schneider. Wiley–VCH, Weinheim, 2001, pp. 79–83.
41. Botier, G., Vicens, J. and Chermant, J. L., Understanding the creep behaviour of a 2.5D C_f–SiC composite. I. Morphology and microstructure of the as-received material. *Mater. Sci. Eng.*, 2000, **A279**, 73–80.
42. Botier, G., Chermant, J. L. and Vicens, J., Understanding the creep behaviour of a 2.5D C_f–SiC composite. II. Experimental specification and macroscopic mechanical creep responses. *Mater. Sci. Eng.*, 2000, **A289**, 265–275.
43. Coath, J. A. and Wilshire, B., Deformation processes during high-temperature creep of lime, magnesia and doloma. *Ceram. Int.*, 1977, **3**, 103–108.
44. Coath, J. A. and Wilshire, B., The influence of variations in composition on the creep behaviour of doloma. *Ceram. Int.*, 1978, **4**, 66–70.